Fatigue Crack Growth Paths in Al-Si-Mg Cast Alloys

Diana A. Lados and Diran Apelian

Worcester Polytechnic Institute, 100 Institute Road, Worcester, MA 01609, USA
lados@wpi.edu, dapelian@wpi.edu

ABSTRACT. *Fatigue crack growth of long and small cracks was investigated for hypoeutectic and eutectic Al-Si-Mg cast alloys. Crack growth behavior in the near-threshold regime and Regions II and III was related to microstructural constituents namely primary α-Al dendrites and volume fraction and morphology of eutectic Si. Long cracks thresholds reflect combined closure effects of global residual stress and microstructure/roughness. The small crack threshold behavior is explained through closure independent mechanisms, specifically through the barrier effects of characteristic microstructural features specific to each alloy. In Regions II and III changes in fracture surface roughness are associated with different crack growth mechanisms at the microstructural scale. The extent of the plastic zone ahead of the crack tip was successfully used to explain the observed changes in crack growth mechanisms.*

1. INTRODUCTION AND BACKGROUND

Cast aluminum components for fatigue critical applications can be designed by either the traditional "safe life" approach (based on stress/strain-life curves) or the "damage tolerant" approach (based on fracture mechanics concepts). Since even high quality cast aluminum components contain porosity, oxides and other inclusions, crack initiation life can be a small fraction of the total life. Therefore, material and process selection for fatigue critical applications should consider fatigue crack growth life.

Damage tolerant designs commonly use "long crack" fracture mechanics calculations. However cracks, especially in early growth stages, are characterized by a "small crack" behavior. At low stress ratios, small cracks propagate at stress intensity ranges below the long crack threshold, ΔK_{th} [1-3], and for similar stress intensities, they propagate at significantly faster rates. Conservative estimates of fatigue life take small crack behavior into account especially in the near-threshold regime (i.e. high cycle fatigue applications).

Small cracks have been classified [2,4] as mechanically small compared to the scale of the local plasticity, microstructurally small compared to relevant microstructural dimensions, and physically small. Microstructurally small cracks exhibit an oscillating growth rate behavior of acceleration followed by retardation. In wrought alloys retardation has been associated with grain boundaries [5,6], while in cast aluminum alloys with secondary microstructural phases such as eutectic Si particles [7,8,9]. Crack closure, a concept introduced by Elber in 1972 [10], has been used to explain the differences between long and physically small cracks. There are various sources of closure: plasticity, oxide or debris, roughness/microstructure, macro residual stress, viscous fluid penetration, phase transformation, etc.; these were reviewed by Taylor [11]. Microstructure/roughness induced closure has been used to explain the near-threshold behavior of cast Al alloys [12-14] and

Al alloy composites [15-17]. Another important source of closure is externally induced residual stress (mainly due to quenching during heat treatment). The significance of global residual stresses in fatigue crack growth, and methods to account for the presence of residual stress have been presented by Lados and Apelian [18].

Closure effects become less significant in Regions II and III, and growth mechanisms are dictated by microstructural features such as secondary dendrite arm spacing (SDAS) [19-23], Si particles (morphology and distribution), Si particle/matrix interface strength [9,23,24].

2. EXPERIMENTAL PROCEDURE

2.1 Materials and Sample Preparation

Five cast Al-Si-Mg alloys with the same Mg content (0.45%) but different Si levels, 1, 7, and 13%, were investigated. The eutectic Si in 7 and 13%Si alloys was studied in both unmodified (UM) and Sr-modified (M) conditions. The eutectic Si was modified using a commercial Al-10%Sr master alloy, and appropriate additions were made for each Si content [14]. The average Si particle size values (in μm) for the eutectic containing alloys are: 2.77 for 7%Si-UM; 2.19 for 7%Si-M; 2.94 for 13%Si-UM; and 2.05 for 13%Si-M. The corresponding shape factors are: 1.41, 1.21, 1.86, and 1.19, where shape factor = $\text{perimeter}^2/(4\cdot\pi\cdot\text{area})$.

A constant SDAS (20-30 μm) was attained in all alloys by controlling the freezing rate in a specifically designed sand mold containing chills. All alloys were grain refined using a commercial Al-5%Ti-1%B master alloy to achieve the same grain size (280-320 μm) irrespective of the Si level and degree of eutectic modification [14].

Two peak-strength T61 heat treatments were applied to all samples: one using a room-temperature water quench and the other using an uphill/reverse quench. The later treatment was designed to minimize residual stress (details on the procedures and residual stress levels can be found in [18]). Despite the significant difference in residual stress, both procedures provided similar microhardness of the α-Al matrix for all alloys (100-105 HV). Tensile properties for all alloys were previously reported [14].

The microstructures of all alloys after heat treatment are presented in Figure 1. Porosity level was less than 0.005% in all alloys, so porosity effects on the crack growth were not significant.

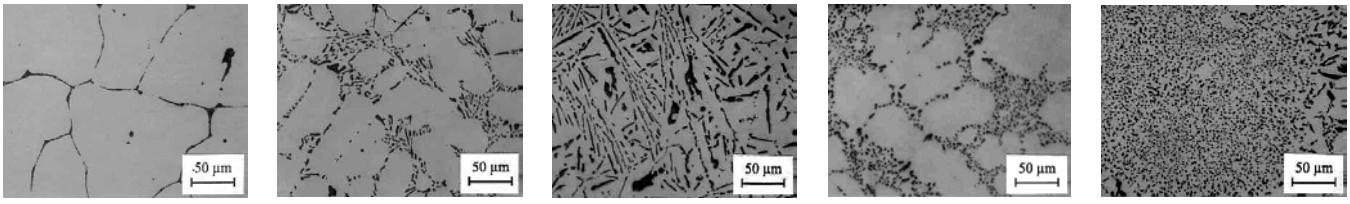

(a) (b) (c) (d) (e)

Figure 1. Alloy microstructures after heat treatment (etched with 1%HF for 10-15 seconds): (a) 1%Si; (b) 7%Si-UM; (c) 13%Si-UM; (d) 7%Si-M; (e) 13%Si-M.

2.2 Testing

Two specimen geometries were designed for the fatigue crack growth work. The long fatigue crack growth was performed on compact tension, C(T), specimens (95 mm × 91 mm × 10 mm) with a notch length of 19 mm measured from the pin holes. The small fatigue crack growth work was done on single corner notched rectangular specimens (10 mm × 10 mm gage cross section area and 23 mm × 10 mm grip cross section area) with a starting triangular corner flaw of ~0.5 mm on each edge. All C(T) specimens were tested under K-control per ASTM E647 at R=0.1, in laboratory air at room temperature 24°C and relative humidity 40-50%. Threshold data were generated under decreasing K, while Regions II and III data under increasing K. Above 10^{-3} mm/cycle, the test was continued using a shallower K-gradient to obtain the steeper Region III data. Further details on the specimen preparation and testing can be found elsewhere [25].

3. RESULTS AND DISCUSSION

3.1 Crack Growth in the Near-Threshold Regime

3.1.1 Long crack growth mechanisms in the near-threshold regime

Experimentally measured long crack threshold values, ΔK_{th}, both for samples with low residual stress (Figure 2(a)) and high residual stress (Figure 2(b)) are higher than the corresponding physically small crack values (Figure 2(c)). The difference is attributed to crack closure since for long cracks part of the applied force is used to reopen the mismatched interfering faces. Thus, the magnitude of the applied stress intensity factor range is reduced, and less cyclic damage occurs at the crack tip. Two important sources of closure are associated with this class of materials [14]: roughness (which is dictated by the alloy's microstructure and it can be quantified by comparing Figures 2(a) and 2(c)) and global residual stress (which is caused by quenching during heat treatment and it can be quantified by comparing Figures 2(a) and 2(b)).

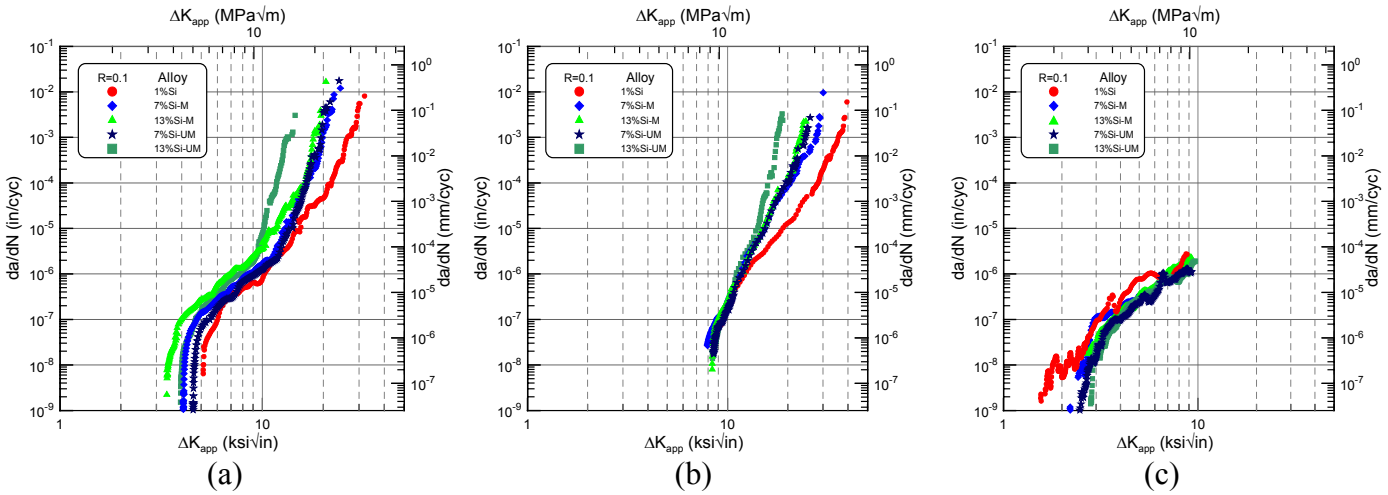

Figure 2. Fatigue crack growth data for 1, 7, and 13%Si cast Al-Si-Mg alloys: (a) long crack data – low residual stress; (b) long crack data – high residual stress; (c) small crack data.

Figure 2(a) shows the effects of Si content and morphology on long crack thresholds, ΔK_{th}. Increases in Si content decrease ΔK_{th}, and Si modification further reduces ΔK_{th}, for both the 7 and 13%Si alloys. The differences in threshold can be explained through the effect of microstructural features on crack deflection, which dictate the fracture surface roughness and thus the level of roughness induced closure, Figure 3 (fractographic observations – top, crack deflection models – bottom). In 1%Si alloys with no eutectic, the crack advances through the α–Al matrix until obstacles such as grain boundaries cause an orientation change. In 7 and 13%Si alloys, eutectic Si particles deflect the crack, thus creating deflection distances smaller than the grain size, less roughness, and lower ΔK_{th}. Roughness values (the distances between the highest peak and the lowest valley averaged over a sequence of successive characteristic areas in the near-threshold regime) are consistent with the long crack threshold ranking and also in direct correlation with the "microstructural characteristic dimension" (MCD) causing crack deflection in each alloy, namely grain size, SDAS, and inter-Si particle distance for 1, 7 and 13%Si alloys, respectively [14].

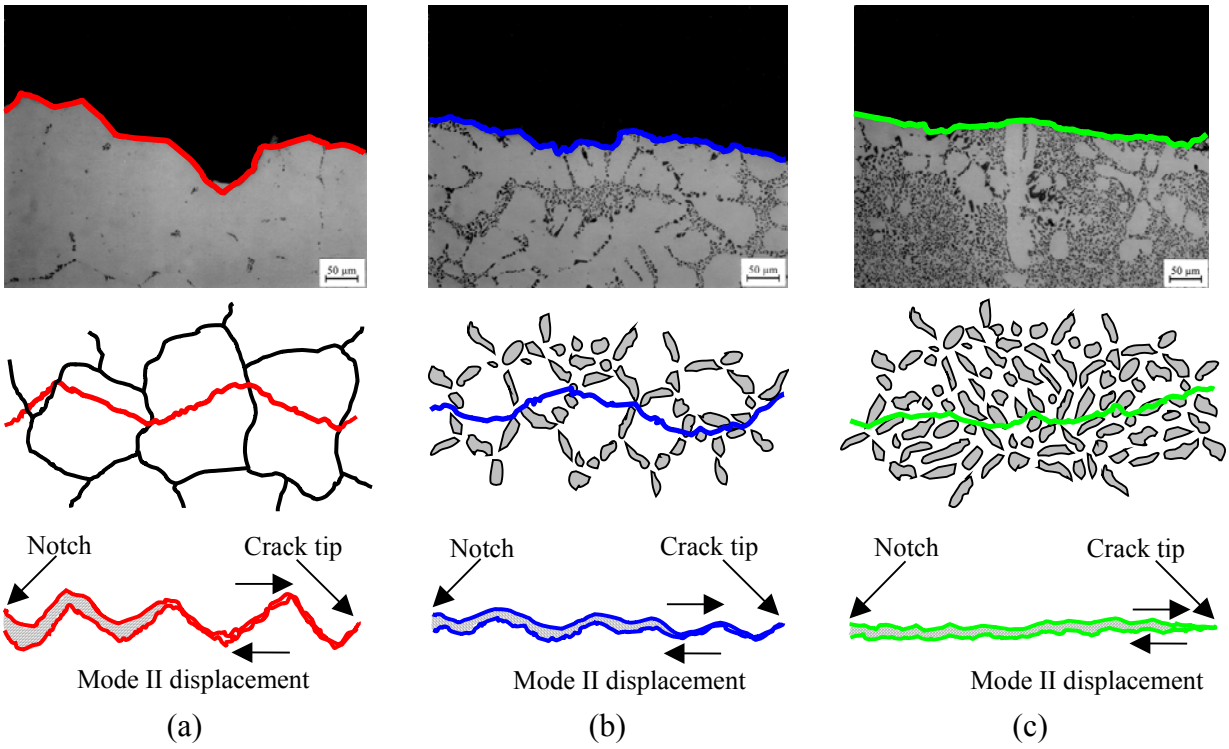

Figure 3. Crack path deflection for three Al-Si-Mg alloys at similar and low ΔK:
(a) 1%Si; (b) 7%Si; (c) 13%Si
(fractographic observations – top and crack path models – bottom).

Unmodified alloys have higher long crack thresholds than modified alloys for both 7 and 13%Si, Figure 2(a). This behavior can be explained through the impact of Si morphology on the crack advance [14]. For the same vol.% Si, Si particles are coarser and more distantly spaced in unmodified alloys (especially in the 13%Si alloys). As a result, in the unmodified alloys, the crack may not always be deflected by Si particles at the edge of the dendrites, and also when the crack debonds or fractures the Si particles, larger deflections are created. Larger deflections generate rougher surfaces, hence more roughness induced

crack closure, and higher ΔK_{th}. Similar differences between unmodified and modified alloys have also been reported in the literature [20].

In the presence of high compressive residual stresses threshold values doubled compared to the corresponding low residual stress values (9-10 MPa√m versus 3.5-5.5 MPa√m, see Figures 2(a) and 2(b)). Thresholds are dominated by residual stress induced closure mechanisms and the material-dependent threshold ranking was lost due to reduced contributions from microstructure/roughness induced closure. For low residual stress samples, the microstructure/roughness induced closure is active near the crack tip and the height/angle of interfering asperities dictate the level of closure. For high residual stress, the crack tip remains open at all times and closure mechanisms become operative near the notch (bulge effect). This change in contact behavior explains the reduced contribution of roughness to total closure since near the notch the roughness differences between various alloys are relatively small compared to the total crack opening displacement (COD). More details can be found in Lados et al. [14].

3.1.2 Small crack growth mechanisms in the near-threshold regime

Different criteria [26,27] have been proposed to define "small crack" sizes (see general guidelines in ASTM E647). However, for a correct mechanistic understanding of the crack growth behavior, the general guidelines must be tailored to the size of the "microstructural characteristic dimensions" (MCD) of Al-Si-Mg alloys [14]. A growing crack is considered mechanically small if its length is in the order of the plastic zone size ($a \approx r_p$); microstructurally small if its length is in the order of the MCD [$a \approx (5 \text{ to } 10) \times MCD$]; and physically small when its length is significantly larger than the MCD ($a >> MCD$). The growth of physically small cracks is similar to that of long cracks except for closure effects. Closure corrective techniques can estimate the physically small crack growth behavior of the material by compensating for closure effects, but cannot predict microstructural effects associated to acceleration/retardation behavior.

The initial crack size in all small crack growth tests was ~500 μm. Due to the differences in microstructural characteristic features and mechanical behavior of the three Si level alloys, a combined microstructural-mechanical assessment was done to determine the initial crack growth stage for each of the alloys. Since the plastic zone size in the near-threshold regime is roughly 5-10 μm, none of the alloys experienced mechanically small crack growth.

To determine whether or not any of the alloys displayed microstructurally small crack behavior, the MCDs for each alloy were established. These were: $MCD_{1\%Si}$ = GS (grain size), $MCD_{7\%Si}$ = SDAS, and $MCD_{13\%Si} = d_{Si\text{-}Si}$ (interparticle Si spacing). At a grain size of 280-320 μm (i.e. $MCD_{1\%Si}$) microstructurally small crack behavior is expected for the 1%Si alloy. The peaks and valleys on the small crack growth curve of this alloy, Figure 2(c), correspond to retardation/acceleration at the grain-boundaries/center-of-the-grains.

For the 7%Si alloys, the initial crack size represents $\approx 20 \times MCD_{7\%Si}$ and thus physically small crack behavior is expected. Thus, the crack complies with the long crack closure corrected growth behavior, a fact confirmed by the absence of oscillating behavior.

For the 13%Si alloys, the initial crack size is two orders of magnitude larger than the $MCD_{13\%Si}$, which corresponds to a significant population of Si particles. Therefore, these alloys also show an initial physically small crack growth behavior.

3.2 Crack Growth in Regions II and III

3.2.1 Crack propagation mechanisms in Regions II and III for 7 and 13%Si alloys

The mechanisms active at different stages during stable crack propagation (Region II) and fast fracture mode (Region III) are discussed with respect to microstructure namely the α-Al matrix strength, the bonding strength at the interface between α-Al structure and eutectic Si particles, and the strength of the Si particles. The following explanations are based on the concept that cracks seek the path of least resistance provided by the most damaged microstructural features ahead of it.

Fracture surfaces roughness increases as the cracks propagate through Region II and into Region III, Figure 4. As an example, for a modified 7%Si alloy, the surface roughness index increased from 1.2 in lower Region II to 1.8 in lower Region III, which corresponds to an increase in crack growth rate from 6.6 to 93 nm/cycle.

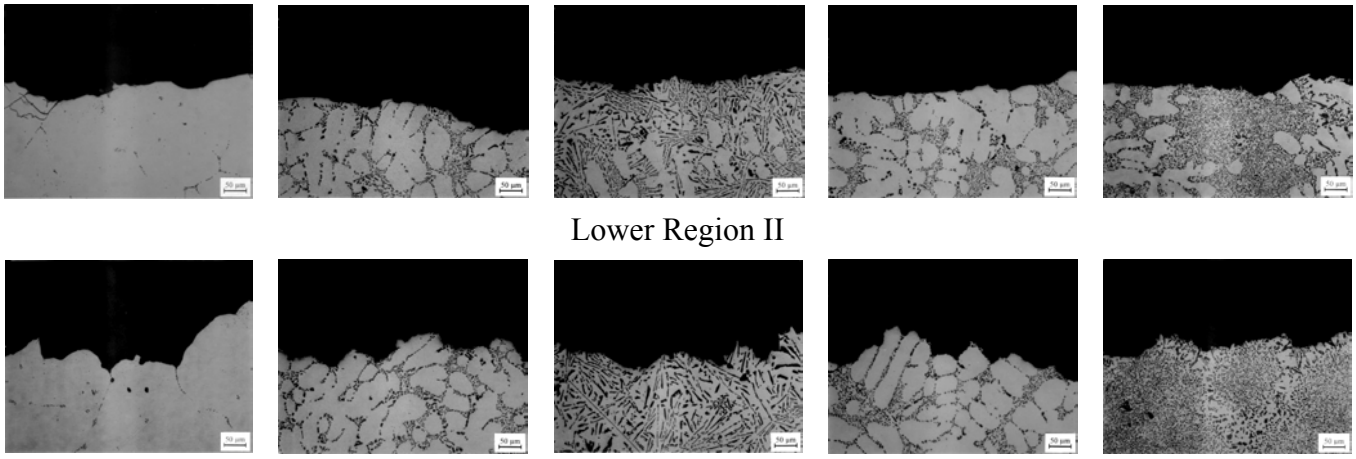

Figure 4. Changes in fracture surface roughness with increasing ΔK from lower Region II (top) to lower Region III (bottom):
(a) 1%Si; (b) 7%Si-UM; (c) 13%Si-UM; (d) 7%Si-M; (e) 13%Si-M.

For the 7%Si alloys, the changes in roughness are associated with a gradual change in propagation mechanisms at the microstructural scale. At low ΔK, the flat fracture surface corresponds to a crack advance through the microstructural constituent found directly ahead of the crack tip: mainly the α-Al structure with occasional encounters with Si particles located straight ahead of the crack tip. With increasing ΔK, fracture surfaces reveal an increasing number of Si particles indicating an increasing crack preference to interact with Si particles. At high ΔK, the crack preferentially advances through Al-Si eutectic regions, and its appearance became increasingly tortuous. A crack's general tendency is to grow normal to the direction of principal stress unless damaged material away from the crack front makes it energetically more favorable to meander. An increasing number of Si particles along the crack path with increasing ΔK and crack length has been previously reported [9,16,17,23].

These mechanistic changes can be explained by considering the amount of damaged material ahead of the crack tip at various ΔK, which can be approximated by the monotonic plastic zone size [28]. An expression for the monotonic plastic zone, Eq. 1, taking into account effects from both plane stain and plane stress was developed [28]. For simplicity the same cardioid shape was assumed for the whole range from plane strain to plane stress, the only difference being in the plastic zone size.

$$r_p \approx \left(\frac{1}{2\pi}\right)^n \left(\frac{1}{6\pi}\right)^{1-n} \frac{K_{max}^2}{\sigma_{YS}^2} \cos^2\frac{\theta}{2}\left(1+3\sin^2\frac{\theta}{2}\right) \qquad (1)$$

where n = degree of plane stress = $\dfrac{1.33 \cdot r_{p(\text{plane-stress})}}{B}$ $\quad 0 < n \le 1$;

The plastic zone radius in Eq. 1 needs to be compared with the critical MCD, which controls the crack advance. For the 7%Si alloys, $MCD_{7\%Si}$ = SDAS~25 μm, signifying that a plastic zone larger than the $MCD_{7\%Si}$ will contain Si particles that have been either damaged or had a weakened interface to provide an easy path for the incoming crack. A plastic zone, r_p~SDAS, corresponds to a crack driving force ΔK ≈ 5.5 MPa√m (5 ksi√in), which is the value near the transition point from near-threshold regime to stable growth in Paris Region II. Crack deflection from Si particles contributing to roughness induced closure in the near-threshold regime [14] transitions to a crack acceleration mechanism as Si decoheres from the matrix in the plastic zone [9,17,23]. At low ΔK, there is not enough strain energy in the plastic zone to fracture Si particles unless the particles have a high aspect ratio and their principal axis perpendicular to the crack plane. In such cases, Si particles have high resistance to debonding due to large interface areas parallel to the loading direction [29], and they are more likely to fracture. It was observed [23] that high aspect ratio Si particles with an inclination angle to the crack plane <45° or >135° have a tendency to debond, Figures 5(a) and 5(d), while particles with angles between 45° and 135° are expected to break, even at low crack driving forces, Figures 5(b) and 5(d). However, when a Si twin plane is parallel to the crack front, Si particles can fracture at angles <45° or >135°, Figure 5(c).

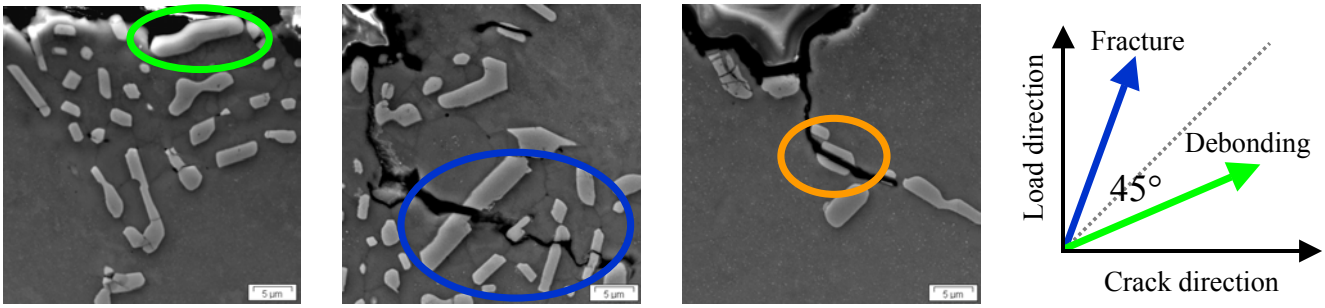

(a) (b) (c) (d)

Figure 5. Failure mechanisms for particles with high aspect ratio:
(a) debonding, (b) fracture, and (c) fracture on twin plane;
(d) Transition from debonding to fracture for high aspect ratio Si particles as a function of particle orientation with respect to load and crack direction.

Figure 6(a) shows the evolution of the plastic zone with increasing crack driving force for a 7%Si alloy [23]. At low ΔK, the plastic zone interacts with only a few Si particles and the amount of Si particles on the fracture surface is low. At ΔK values between 5 and 9 MPa√m (4.5 and 8 ksi√in), Figure 6(a)-left, the crack advances through the damaged dendritic structure; when Si particles with weakened interfaces/structures are encountered near the crack tip, the crack follows the weaker path provided by the Si. As ΔK increases, the number of Si particles on the fracture surface increases, reflecting the crack's preference for advancement via Si particles. For the crack to exclusively follow Si particles, a continuous path of debonded or cracked Si particles in the plastic zone ahead of the crack tip is required. In this case, it becomes energetically more favorable for the crack to deviate from the planar advancement and meander through the regions of least resistance. In lower Region II, the crack interacts with individual particles, then, at ΔK>8-9 MPa√m (7-8 ksi√in), Figure 6(a)-middle, it follows a sequence of Si particles primarily located on the cell boundaries not too far from the main crack direction. As ΔK further increases, at ΔK>11-12 MPa√m (10-11 ksi√in), Figure 6(a)-right, the roughness increases, a plastic zone large enough to damage one or more complete Al-Si eutectic region(s) is reached, and a continuous network of damaged Al-Si eutectic colonies becomes available to the crack. This propagation mode occurs near the transition from Paris regime to Region III of fast growth. At high ΔK, when the plastic zone is large and the cumulative strain damage is high, the number of fractured Si particles increases even in the modified structures, and cracks propagate via both debonding and fracture mechanisms.

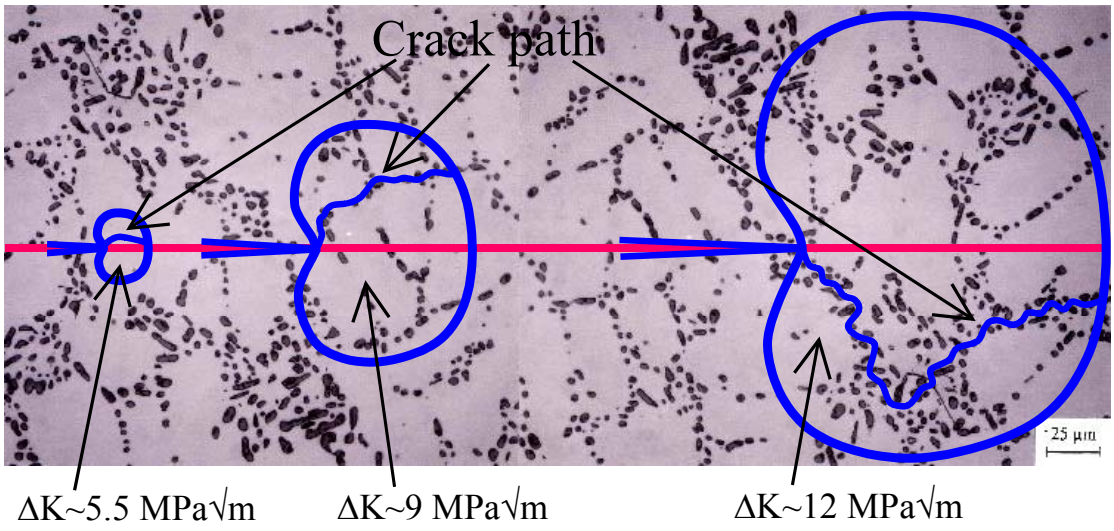

Figure 6. Plastic zone size at the microstructural scale of a 7%Si alloy for different ΔK.

Crack behavior in Region III is characterized by fast crack growth exclusively following eutectic regions. The overload fracture in upper Region III occurs almost entirely through ductile static tearing of the large Al-Si eutectic regions. As a result, pseudo-fracture toughness (highest ΔK value) is mainly dictated by the Si particle morphology. Thus, the coarse/irregular Si morphology provides convenient paths for the crack to debond or cut through, while the modified Si morphology exerts more resistance to crack growth, as the particles are more fracture resistant. Modified 7%Si alloys show slightly improved behavior in Region III compared to unmodified alloys, but the effect of modification is more

pronounced in the case of 13%Si alloys. Thermal modification during heat treatment minimizes the differences in Si morphology between unmodified and modified alloys. However, the large plates in 13%Si alloys require a longer time to fragment and spheroidize, and preservation of the plate-like structure in the unmodified alloys drives larger differences between the high ΔK crack growth behavior of unmodified and modified 13%Si alloys. Larger differences in pseudo-fracture toughness are caused by larger differences in Si morphology, which is a function of Si content, modification, solidification conditions, and heat treat time. The Si morphology ranking is in perfect agreement with the fracture toughness ranking for the Si containing alloys. Results of this study agree with the literature for A356 [20,30] and Al-12%Si-0.35%Mg [24] alloys.

The monotonic material failure in upper Region III and toughness values are strongly dependent on the Si morphology and less on the Si content, Figure 2(a). The modified alloys with 7 and 13%Si have similar toughness values due to a similar Si morphology while the unmodified alloys show a toughness shift equivalent to the Si morphological differences. To predict toughness, model equations based on the size and the shape of the Si particles are needed: ΔK_{FT} = f (Si shape, Si size, Si distribution, Si content).

3.2.2 Crack propagation mechanisms in Regions II and III for 1%Si alloys

In the alloys, which do not contain eutectic Si (i.e., 1%Si), the crack growth mechanisms change from transgranular to intergranular [23], as seen in Figure 7. In these alloys, the crack preferentially selects the damaged grain boundaries in the plastic zone. With increasing ΔK, the plastic zone grows until it becomes sufficiently large to facilitate propagation exclusively along grain boundaries. For these alloys grain size becomes the controlling parameter in fatigue crack growth, similar to wrought alloys.

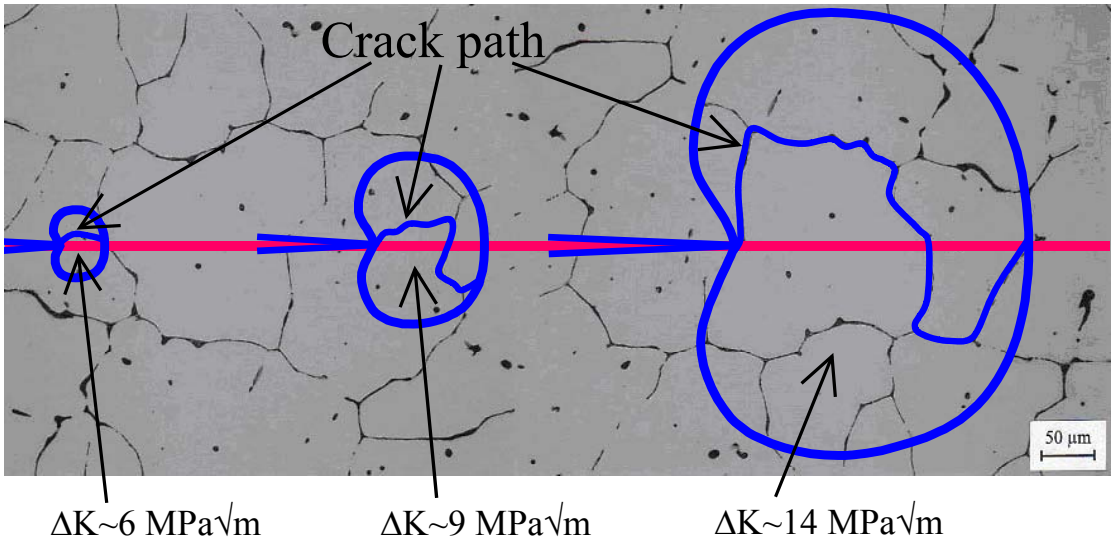

Figure 7. Crack path with increasing ΔK for cast alloys with no/low eutectic phase (transgranular left and intergranular right).

4. CONCLUSIONS

1. The near-threshold long crack growth behavior of the Al-Si-Mg alloys studied is dominated by closure mechanisms.
2. At low residual stress levels, the effect of microstructure is evident and the long crack thresholds, ΔK_{th}, are inversely proportional to the vol% eutectic Si.
3. As a general trend, higher thresholds and lower near-threshold growth rates are achieved for coarser microstructures, which result in rougher fracture surfaces, and higher closure.
4. The near-threshold small crack growth behavior is strongly dependent on the alloy's unique "microstructural characteristic dimension" (MCD).
5. Physically small cracks are less microstructurally sensitive and they behave similarly to the long cracks except for the absence of closure. Closure corrective methods can be used to estimate the physically small crack growth behavior from long crack growth data, but they do not to capture microstructure effects.
6. With increasing ΔK from lower Region II to upper Region II and Region III, an increase in fracture surface roughness is observed. The increase in roughness is associated with a change in fatigue crack growth mechanisms from a predominant crack advance through the primary α-Al matrix to an exclusive growth around/along/through Si particles and eutectic regions.
7. The changes in mechanism can be explained using correlations of the plastic zone size at various ΔK levels with the microstructural features enveloped by it, which provide a weak link in front of the crack.
8. Fracture toughness is mainly a function of the size and the shape of the Si particles: ΔK_{FT} = f (Si shape, Si size, Si distribution, Si content).
9. In the alloys with no eutectic Si (1%Si), grain size shows an effect similar to the one observed in wrought alloys, and it represents the controlling dimension governing the crack growth.

References

1. Miller, K.J. (1982) *Fatigue Fract. Eng. Mater. Struct.* **5**, 223-232.
2. Suresh, S., Ritchie, R.O. (1984) *Int. Met. Rev.* **29**, 445-476.
3. Lankford, J. (1982) *Fatigue Fract. Eng. Mater. Struct.* **5**, 238-248.
4. Ritchie, R.O., Lankford, J. (1996) *Mater. Sci. Eng.* **84**, 11-16.
5. Tanaka, K. (1987). In: *Small Fatigue Cracks*, pp. 343-361, Ritchie, R.O. and Lankford, J. (Eds.), The Metallurgical Society, Warrendale, PA.
6. de los Rios, E.R., Navarro, A. (1990) *Phil. Mag. A.: Phys. Condens. Matter. Defects Mech. Prop.* **61**, 435-449.
7. Shiozawa, K., Tohda, Y. and Sun S.-M. (1997) *Fatigue Fract. Eng. Mater. Struct.* **20 (2)**, 237-247.
8. Plumtree, A., Schafer, S. (1986). In: *The Behavior of Short Fatigue Cracks*, pp. 215-227, Miller, K.J., and de los Rios, E.R. (Eds.), Mechanical Engineering Publications, London, UK.
9. Gall, K., Yang, N., Horstemeyer, M., McDowell, D.L., and Fan, J. (1999) *Metall. Mater. Trans.* A **30A**, 3079-3088.

10. Elber, W. (1971). In: *Damage Tolerance in Aircraft Structures, ASTM STP 486*, pp. 230-242, American Society for Testing and Materials, Philadelphia, PA.
11. Taylor, D. (1988) *Int. J. Fatigue* **10**, 67-79.
12. Kubota, M., Ochi, Y., Ishii, A., and Shibata, R. (1998) *Mater. Sci. Research Int.* **4 (3)**, 193-199.
13. Kumai, S., Sekikawa, A., Hu, J., Higo, Y., and Nunomura, S. (1995) *J. Jap. Inst. Light Metals* **45 (4)**, 204-208. (in Japanese)
14. Lados, D.A., Apelian, D. and Donald, J.K. (2006) *Acta Mater.* **54 (6)**, 1475-1486.
15. Kumai, S., Hu, J., Higo, Y. and Nunomura, S. (1996) *Acta Mater.* **44 (6)**, 2249-2257.
16. Shang, J.K., Yu, W. and Ritchie, R.O. (1988) *Mater. Sci. Eng. A* **A102**, 181-192.
17. Sugimura, Y., Suresh, S. (1992) *Metall. Mater. Trans. A* **23A**, 2231-2242.
18. Lados, D.A., Apelian, D. (2006) *Metall. Mater. Trans. A* **37A**, 133-145.
19. Kumai, S., Hu, J., Higo, Y. and Nunomura, S. (1995) *J. Jap. Inst. Light Metals* **45 (4)**, 198-203. (in Japanese)
20. Kumai, S., Aoki, S., Han, S.-W. and Sato, A. (1999) *Mater. Trans., JIM,* **40 (7)**, 685-691.
21. Caton, M.J., Jones, J.W., Boileau, J.M. and Allison, J.E. (1999) *Metall. Mater. Trans. A* **30A**, 3055-3068.
22. Chan, K.S., Jones, P. and Wang, Q. (2003) *Mater. Sci. Eng. A* **A341**, 18-34.
23. Lados, D.A., Apelian, D. and Major, J.F. Fatigue Crack Growth Mechanisms at the Microstructure Scale in Al-Si-Mg Cast Alloys: Mechanisms in Regions II and III, Metall. Mater. Trans. A (2006) (in press).
24. Lee, F.T., Major, J.F. and Samuel, F.H. (1996) *AFS Trans.* **104**, 785-795.
25. Lados, D.A., Apelian, D., Paris, P.C. and Donald, J.K. (2005) *Int. J. Fatigue* **27 (10-12)**, 1463-1472.
26. Ritchie, R.O., Lankford, J. (1987) In: *Small Fatigue Cracks*, pp. 343-361, Ritchie, R.O. and Lankford, J. (Eds.), The Metallurgical Society, Warrendale, PA.
27. *Short fatigue cracks*, *ESIS 13* (1992) Miller, K.J. and de los Rios, E.R. (Eds.), Mechanical Engineering Publications, London, UK.
28. Lados, D.A., Apelian, D. (2006) *Eng. Fract. Mechanics* **73 (4)**, 435-455.
29. McClung, R.C., Sehitoglu, H. (1989) *Eng. Fract. Mechanics* **33**, 237-271.
30. Dighe, M.D., Gokhale, A.M. (1997) *Scr. Metall.* **37**, 1435-1440.